electronics

MDPI

Article

A Current Monitor System in High-Voltage Applications in a Range from Picoamps to Microamps

Rabí Soto-Camacho [1], Sergio Vergara-Limon [1,2], María Aurora Diozcora Vargas-Treviño [1,2]*, Guy Paic [3], Jesús López-Gómez [4], Marciano Vargas-Treviño [5], Jaime Gutierrez-Gutierrez [5], Fermín Martínez-Solis [4], Miguel Enrique Patiño-Salazar [3] and Victor Manuel Velázquez-Aguilar [6]

1 Facultad de Ciencias de la Computación, Benemérita Universidad Autónoma de Puebla, Boulevard 14 Sur and Avenida San Claudio, Ciudad Universitaria, Jardines de San Manuel, C. P. 72570 Puebla, Mexico; rabi87_soto22@hotmail.com (R.S.-C.); sergio.vergara@correo.buap.mx (S.V.-L.)
2 Facultad de Ciencias de la Electrónica, Benemérita Universidad Autónoma de Puebla, Boulevard 18 Sur and Avenida San Claudio, Ciudad Universitaria, Jardines de San Manuel, C. P. 72570 Puebla, Mexico
3 Instituto de Ciencias Nucleares, Universidad Nacional Autónoma de México, Avenida Universidad, Delegacion Coyoacán, C. P. 04510 Ciudad de México, Mexico; guypaic@nucleares.unam.mx (G.P.); mpatino960@hotmail.com (M.E.P.-S.)
4 Ingeniería Eléctrica y Electrónica, División Académica de Ingeniería y Arquitectura, Universidad Juárez Autónoma de Tabasco, Avenida Universidad s/n, Zona de la Cultura, Colonia Magisterial, C. P. 86040 Villahermosa Centro, Mexico; jesus.lopezg@ujat.mx (J.L.-G.); fermin.martinez@ujat.mx (F.M.-S.)
5 Escuela de Sistemas Biológicos e Innovación Tecnológica de la Universidad Autónoma "Benito Juárez" de Oaxaca, Avenida Universidad S/N, Ex-Hacienda 5 Señores, C. P. 68120 Oaxaca de Juárez, Mexico; mvargas.cat@uabjo.mx (M.V.-T.); jgutierrez.cat@uabjo.mx (J.G.-G.)
6 Facultad de Ciencias, Universidad Nacional Autónoma de México, Avenida Universidad, Delegacion Coyoacán, C. P. 04510 Ciudad de México, Mexico; vicvela@ciencias.unam.mx
* Correspondence: aurora.vargas@correo.buap.mx

Abstract: In this article, we present a system to measure current in the range of 0 to 10 μA with high-voltage isolation up to 5 kV. This current monitor consists of three ammeters connected in series, to improve the resolution in the measurement. The design features several innovative elements such as using low voltage to provide power to the devices to measure the current and digitize it with a sampling frequency of 1 KHz, it is generated based on a DC-DC converter that produces three voltages, +12 V, −12 V, and 5 V, from a conventional 10 V source. The three voltages are referenced to the same floating ground. The DC-DC converter has a high voltage insulation up to 5 kV and four optocouplers with an insulation up to 20 kV are used to read the digitized data. The introduction of a DC-DC converter contributed to reduce the noise level in the analog part of the circuit which has been resolved implementing shields inside the board. In particle physics, several systems are used to detect particles in high-energy physics experiments such as Gas Electron Multiplier (GEM), micromegas, etc. GEMs suffer small deteriorations due to discharges in constant operation and require monitoring the current consumption at high frequency (1 kHz). In this work, we present the design and operation of a 0 to 10 μA auto scale ammeter. The results obtained by monitoring the current in a 10 × 10 cm^2 GEM are shown.

Keywords: autoscale ammeter; current monitoring; data acquisition system; electromagnetic interference; electronics; gas electron multiplier

Citation: Soto-Camacho, R.; Vergara-Limon, S.; Vargas-Treviño, M.A.D.; Paic, G.; López-Gómez, J.; Vargas-Treviño, M.; Gutierrez-Gutierrez, J.; Martínez-Solis, F.; Patiño-Salazar, M.E.; Velázquez-Aguilar, V.M. A Current Monitor System in High-Voltage Applications in a Range from Picoamps to Microamps. *Electronics* **2021**, *10*, 164. https://doi.org/10.3390/electronics10020164

Received: 13 December 2020
Accepted: 10 January 2021
Published: 13 January 2021

1. Introduction

In high energy physics, several detectors have played a very important role in the study of particles produced by colliding ions. One of these is the gas-based electron multiplier (GEM) used for the detection of produced particles, such as [1,2]. Chernyshova et al. in [3] presented an application of a GEM detector in the development of a tungsten-level monitoring system in ITER of the WEST tokamak project. A.F. Buzulotskov in [4] presented

its use in radiation systems. A complete X-ray fluorescence spectroscopy (XRF) imaging system based on a standard 10 cm × 10 cm 3-stage gas electron multiplier (GEM detector) was presented in [5]. As well as works related to the Gas Electron Multiplier (GEM) detector soft X-ray spectroscopy system for tokamak applications used GEM detector has one-dimensional, 128-channel readout structure, reprocessing algorithms are implemented in the FPGAs in which the scope of the work is an FPGA-based implementation of the recorder of the raw signal from GEM detector [6,7]. FPGA and Embedded System-Based Fast Data Acquisition and Processing for GEM detectors [8] are used for detection of ionizing radiation and Gas electron multiplier (GEM) detectors from the works [4,9].

In operation, small discharges are generated that can deteriorate the material of the GEMs. These discharges have been documented in the literature. A. Deisting et al. in [10] studied the secondary discharges that occur in a GEM detector in normal operation. The authors presented a mitigation proposal by means of the use of resistors connected in series to the voltage source. Utrobicic et al. in [11] presented the study of delayed discharges that occur in a GEM. These discharges in the detectors can damage the material, requiring the monitoring of the current consumption in GEM detectors at very short time interval order of 1ms. Deyang Yu et al. in [12] presented the design of a picoammeter for application in measurements of charged particle beam current distribution based on the use of instrumentation amplifiers.

The design of a floating nanoammeter for the measurement of small currents in high-voltage systems and its communication system based on optical fiber was presented in [13]. Chao et al. [14] presented an accurate low current measurement circuit following a Faraday cup which was developed to monitor the beam current at pA range that consisted of a picoammeter with a bandwidth of 1 kHz and a gated integrator (GI). A. Utrobicic et al. in [15] describe a floating nanoammeter used for monitoring gas detector discharge micropatterns (GEM), which consists of 16 channels, a 16-bit ADC, a lithium battery, and a 1 kHz readout. Its operating range is 0–125 nA with a resolution of 6.5 pA. An FPGA processes data from several nanoammeters which are transferred through optical fiber and sent to the PC by means of a USB 2.0 connection.

Some of the GEM applications are in ultrafast soft x-ray plasma diagnostics using small pick-up pads (pixels) in the read-out plane; the detector can achieve unambiguous two-dimensional imaging of soft X-rays at rates up to 4 MHz/pixel. This type of detector is in development for plasma diagnostics at Tokamak fusion machine [16]. Developing a device capable of on-line control and verification of the radiation treatment of cancer patients is of critical importance. It consists of two consecutive detectors in the same gas vessel, one optimized for keV and the other for MeV photon detection. It is being developed by a group at Karolinska Institute and Royal Institute of Technology, Stockholm [17]. The design of x-ray polarimeter for astrophysics that consist in a single GEM detector with small pads readout provides good efficiency for detection of soft X-rays, and sufficient accuracy to measure the average angle of emission of the emitted photoelectron [18].

In the aforementioned works, in some cases, the use of batteries to generate floating ground is not pertinent, because they need to be changed some time and, depending of the application, the detector and the current monitor are not easily reachable for example in high energy physics experiments in large spectrometers. Therefore, the proposal designed in this work for high energy applied research has not been reported in the scientific literature, and in some cases, the structure they present is different from that of this study in which will be a matter of interest for researchers.

This paper presents a system to monitor the current within three levels autoscaled from 0 to 10 µA with high-voltage insulation up to 5 kV collecting data at a sampling frequency of 1 kHz. The current monitor consists of three ammeters of different ranges, the first from 0 to 90 nA, the second from more than 90 nA to 900 nA, and the third from more than 900 nA to 10 µA. Depending on the current, the adequate scale is automatically selected. The main contributions of this work are the following.

- The use of optocouplers to transmit digital signals between the ADC and the FPGA with high-voltage insulation.
- Some techniques are implemented to reduce electromagnetic interference (EMI) by using vias around ground semi-planes, capacitors connected between supply voltage (VCC) and ground to produce low impedance points for alternative current signals.
- The above allows the use of a DC-DC converter powered by a conventional 10 V power supply, to generate three voltages +12 V, −12 V, and +5 V, referenced to the same floating ground, instead of using batteries.
- A current monitoring system that can change scale automatically.
- A new array of resistors and diodes to protect the amplifier and ADC from discharges.

A current monitor on a GEM is required to observe the deterioration of the detector, and the currents of a new GEM can range from hundreds of pA to nA and as the detector degrades its current can be of the order of microampere. The current consumption of the GEM is a function of its active area. The ammeters proposed above use batteries to reduce noise and operate in a fixed range, so the battery must be changed every so often. In this proposed design, the power of the ammeters is provided by a conventional C.D power supply, and it can also provide an automatic scale change that allows more accurate measurements at small current values. This manuscript is structured as follows. In the first part, the description of the current monitoring system is presented, continuing with the prototype of the current monitor, the experimental results, and finally the conclusions.

2. Design of the Current Monitor

The system to monitor the current is described in Figure 1. It consists of three ammeters connected in series, each one covering the optimum range to optimize the resolution of the instrument. These ammeters use the following scales: 0 to 90 nA, more than 90 nA to 900 nA, and more than 900 nA to 10 μA. The current monitor is connected in series between the high voltage source and the GEM detector. The current reading from each ammeter is achieved using a Cyclone® III FPGA Chip EP3C10F256C on a self-developed board. Inside the FPGA there are 5 firmware modules that consist of instruction blocks for specific purposes. The first block supplies the signals to the ADC to read out the current value from the selected ammeter. To carry out this task it needs to receive the command and the corresponding channel. The second block deserializes the data coming from the ADC selected, and the third block receives a 17-bit word and fixes the scale as a function of the current value. The selection of the ammeter channel is achieved in the following way: the current value of the first ammeter is read, if the reading is between 0 and 90 nA then the current value is a "Data valid"; however, if the measured current is more than 90 nA, the first ammeter goes into saturation so the scale change is made and the second ammeter is read. If the current value is more than 90 nA to 900 nA, the reading data become "Data valid", if the current value is more than 900 nA, the second ammeter goes into saturation so the scale change is made and the third ammeter is read, and this current value would be "Data valid". This block also counts the time to provide a "Data valid" each millisecond. The saturation current of the first ammeter is 100 nA, the saturation current of the second ammeter is 1 μA, and the saturation current of the third ammeter is 10 μA. The three ammeters are continuously in operation, their values are read, and the comparison of these values is carried out by the FPGA to obtain a "Data valid", this is done for every sample. The Data valid is presented as input of the fourth block to obtain the data format to be sent. The resulting 32-bit word is placed at the input of the fifth block where the corresponding protocol is generated to send the information between the firmware to a computer software via the RN-XV module by Roving Networks® from Silicon Valley, West Coast, CA, USA, with the WiFly device RN-171. It should be noted that a single conventional 10 V, 1 A source is used to power the three ammeters.

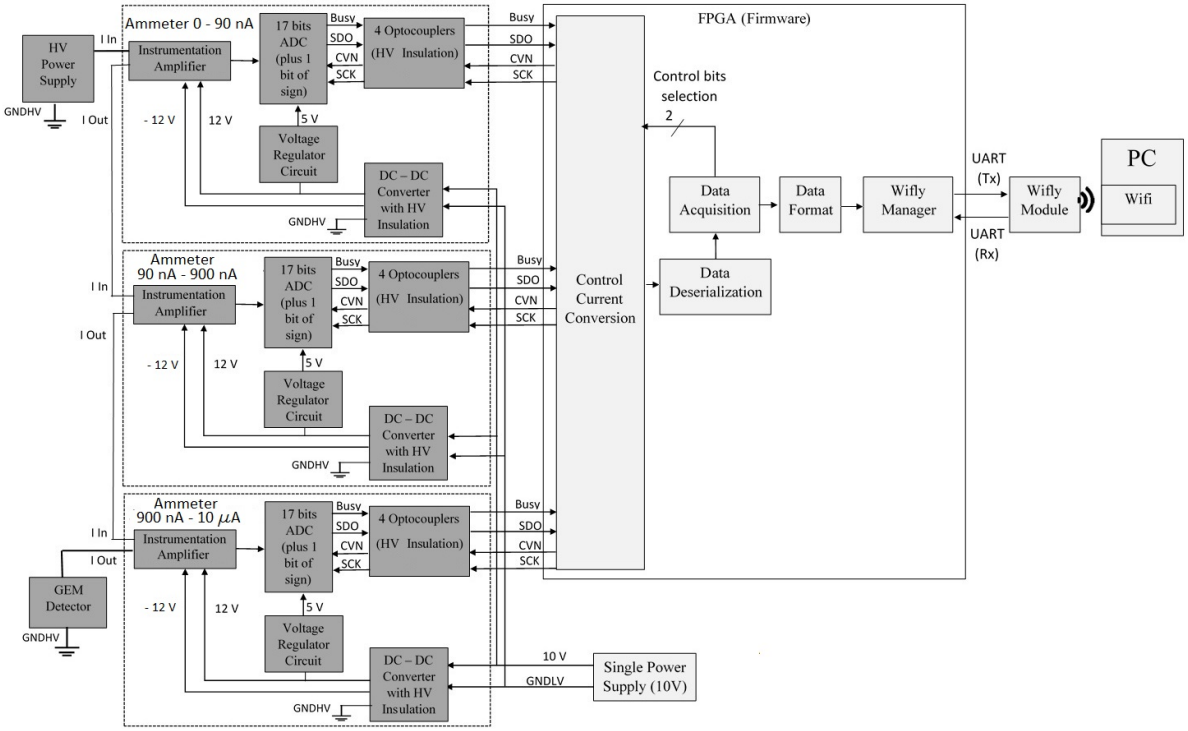

Figure 1. Block diagram of the current monitor.

The instrument is easily scalable if it is necessary to connect more ammeters to cover a wider range; the limitation depends on the number of terminals available on the FPGA board and the modification of the FPGA control firmware would be a simple task. Each ammeter consists of a voltage source with a floating ground through a MED-FS16U-1512D DC-DC converter, a 17-bit LTC2326-18 ADC plus 1 sign bit to read data at a rate of 1 kHz, and four OPI1268S optocouplers with high-voltage insulation up to 20 kV. The three ammeters are identical using the same Printed Circuit Board (PCB) design, it is presented in Figure 2.

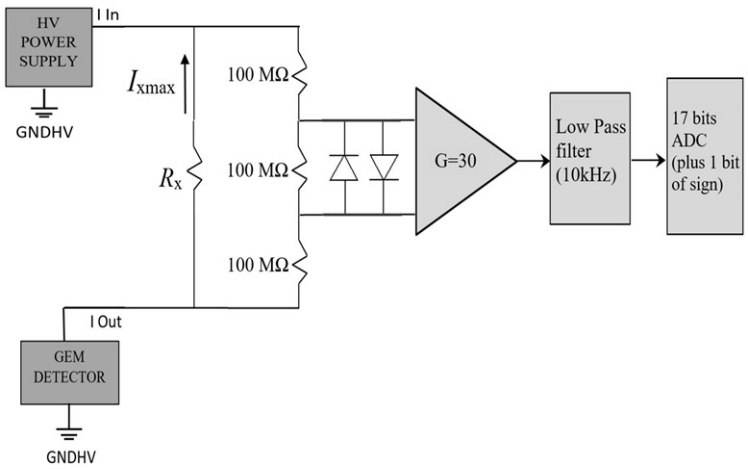

Figure 2. Array of resistors and diodes used to protect ammeters from short circuit.

The scale depends on the value of a single resistor. To protect the amplifier and the ADC from short circuits in the detector a resistive array is implemented, which consists of a resistance R_x connected in parallel to 3 resistors of 100 MΩ in series. In this way the protection of the current monitor is secured. The current produces a voltage of $V_x = I_m R_x$, resulting in a voltage $V_x/3$ at the entrance of the amplifier. The value of V_x is limited to 1 V. Therefore, the maximum voltage through the 100 MΩ resistor connected to the input of the

amplifier is limited to 0.33 V in normal operation. This voltage is smaller than the direct polarization voltage of the protecting diodes. In case of accidental short circuits that would result in applying the full voltage to the resistances the sequence of events is the following: the R_x of 1 W would burn while the three 100 MΩ resistors resist the load. In that case the diodes, depending on the polarization, effectively limit the voltage seen by the amplifier to +/−0.7 V, resulting in an amplifier saturation output voltage of +/−10.5 V.

3. Prototype of the Current Monitor

The main components of the current monitor used for the prototype in this work are presented in Table 1.

Table 1. Main components of the current monitor prototype.

Part	Model/Serie
DC-DC converter	MED-FS16U-1512D
18 bits ADC	LTC2326
Optocouplers	OPI1268S
Instrumentation Amplifier	AD8220
Voltage regulator circuit	TPS75501
FPGA Chip	Cyclone III- EP3C10F256C
Operational Amplifier	MAX999
WiFly module	RN-XV-171

For the design of the PCB, several techniques were implemented to reduce the levels of electromagnetic interference (EMI). These strategies were the segmentation of the ground planes for the high (GND HV) and low voltage (GND LV), the use of vias around these planes, and the use of 100 nF capacitors between the power supply and ground terminals. The purpose of the vias is to form a shield to attenuate the EMI from the digital signals of the ADC and the DC-DC converters to the analog part of the circuit. Each plane shown in Figure 3, where the planes (a–f) are connected to the high-voltage ground (GND HV) and the planes (g,h) are connected to the low-voltage ground (GND LV).

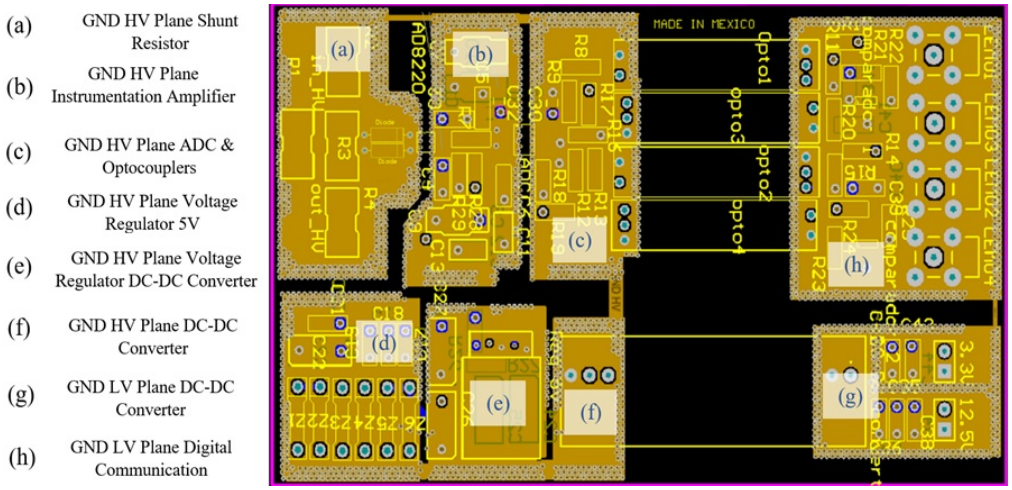

Figure 3. Distribution of the ground planes. The 6 planes (**a**–**f**) to the left of the Printed Circuit Board (PCB) are connected to the high-voltage ground and the planes (**g**,**h**) to the right of the PCB are connected to the low-voltage ground.

The scale resistor R_x, the protection circuit by the three 100 MW resistors, and the diodes are placed on top plane (a). The instrumentation amplifier is mounted between planes (a,b), in order to reduce EMI, and a low-pass filter of 10 kHz is mounted on plane (b). Four signals are used to drive the ADC from the FPGA. To isolate the FPGA from high voltage, 4 optocouplers are used to send and receive the 4 signals. The optocouplers are

located on the bottom between plane (c,h). The low voltage power supply for the DC-DC converter is mounted on the top plane (g). The DC-DC converter is mounted on top between planes (g,f), the +/−12 V outputs of the DC-DC converter are on top plane (f), and finally the voltage regulator circuit that produces the +5 V is mounted on the top planes (d,e). All the ground planes (GND HV) are connected by a narrow trace in order to reduce the EMI between these planes, in the same way, all the planes (GND LV) are connected by a narrow trace too, Figure 3 are illustrated. Furthermore, vias were distributed around each ground plane to produce an electromagnetic shield in order to reduce EMI among all the planes as shown in Figure 4a. Figure 4b presents the components mounted on the top layer of the PCB. The optocouplers are mounted on the bottom layer of the PCB. On the other hand, the PCB design was made in ALTIUM DESIGNER® software following the IPC-2221B and IPC-9592B standard regulations for high-voltage design.

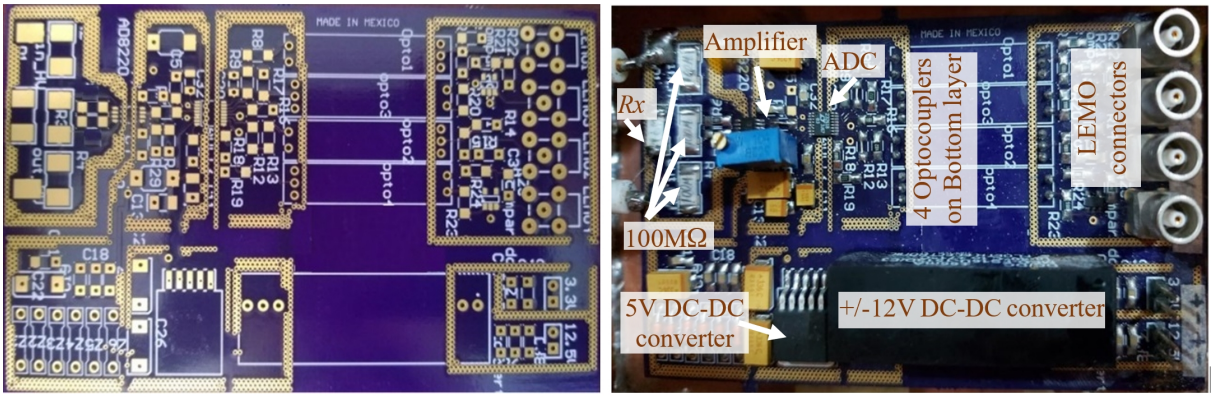

(a) (b)

Figure 4. Photo of the PCB. (**a**) PCB without components and (**b**) PCB with components mounted.

To receive the data and process them, an own interface was developed using the NI LabVIEW™ software, such as in the left side of Figure 5, which displays the data in real-time in the graph, and the right side displays the smoothed data obtained averaging in succession using the last 40 samples taken in real-time. We used NI LabVIEW™ for this work because it is possible to build a user interface simultaneously during the development of the program. Although, likewise, the program can be developed in any other software. NI LabVIEW™ is a commercial software but it has the advantage of allowing to compile the program and produce an executable file (.exe) which can be run on any computer without the need to have NI LabVIEW™ installed. The WiFly module allows the data reading to be transmitted in real-time to the PC via WiFi. However, the module has the option to send the data reading in real-time over the Internet so it can be stored in a cloud or shared with some other device, even though the data could be visualized in an app for mobile devices or on a website.

The calibration of the ammeters was carried out separately, each one according to its scale as can be seen in Figure 6. The three ammeters were connected in series within the current monitoring system. The experimental setup uses a variable power supply connected in series with a commercial ammeter, Keithley® 6514 certified from Aurora Road, Cleveland, OH, USA; in which the instrument is calibrated and accredited by the DIN/ ISO 17025:2005, DIN/ISO 17025:2017 and performs the work in accordance with its quality requirements and national standard ANSI/NCSL Z540-1-1994 (R2002) in the field of calibration [19]. This device is connected in series with the R_x resistor scale included in the corresponding ammeter.

The calibration procedure of the ammeters is the following. Current was made to flow through the resistance R_x of a single ammeter and, simultaneously, this current **I**(nA) was measured including its uncertainty Δ**I**(nA) with the commercial Keithley® 6514 certified from Aurora Road, Cleveland, OH, USA. Therefore, this procedure is repeated for each ammeter, one at a time. To produce this current, it is used a power supply, its voltage was

varied at regular intervals from 0 to 0.99 V with steps of 0.05 V, generating 21 experimental points for each ammeter, as shown in Table 2.

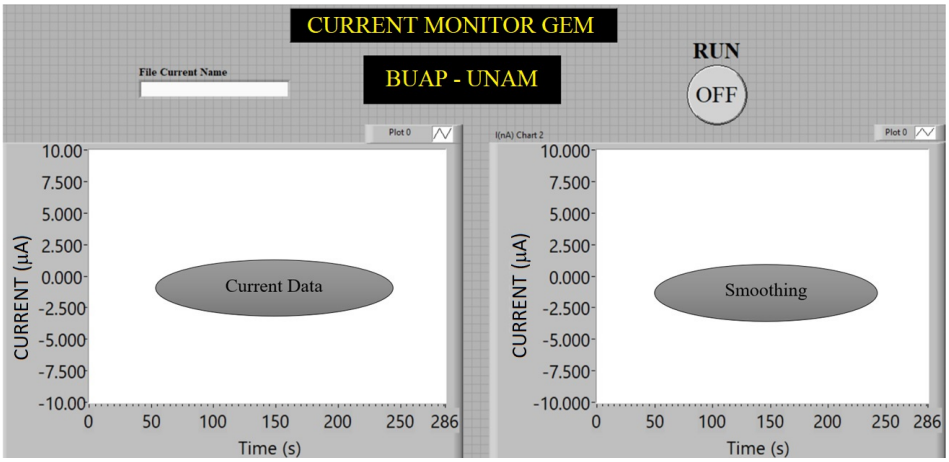

Figure 5. User interface of the current monitoring system.

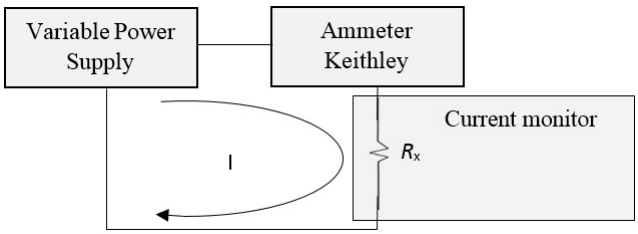

Figure 6. Experimental setup to calibrate the ammeters.

Table 2. Experimental data.

Power Supply	Ammeter 1:	(0–100 nA)	Ammeter 2:	(0–1 μA)	Ammeter 3:	(0–10 μA)
Voltage (V)	**I (nA)**	**Δ I (nA)**	**I (nA)**	**Δ I (nA)**	**I (μA)**	**Δ I (μA)**
0	0	0	0	0	0	0
0.05	5.092	0.0102	50.10	0.1002	0.5315	0.0005
0.10	10.246	0.0205	100.20	0.2004	1.0820	0.0011
0.15	15.174	0.0303	150.30	0.3006	1.5070	0.0015
0.20	20.155	0.0403	200.40	0.4008	2.0060	0.0020
0.25	25.063	0.0501	250.50	0.2505	2.5160	0.0025
0.30	30.237	0.0605	300.60	0.3006	3.0110	0.0030
0.35	35.211	0.0704	350.70	0.3507	3.5090	0.0035
0.40	40.187	0.0804	400.80	0.4008	4.0830	0.0041
0.45	45.025	0.0901	450.90	0.4509	4.5060	0.0045
0.50	50.206	0.1004	501.00	0.5010	5.0240	0.0050
0.55	55.169	0.1103	551.10	0.5511	5.5480	0.0055
0.60	60.107	0.1202	601.20	0.6012	6.0430	0.0060
0.65	65.124	0.1302	651.30	0.6513	6.5010	0.0065
0.70	70.021	0.1400	701.40	0.7014	7.0060	0.0070
0.75	75.092	0.1502	751.50	0.7515	7.5040	0.0075
0.80	80.043	0.1601	801.60	0.8016	8.0030	0.0080
0.85	85.061	0.1701	851.70	0.8517	8.5084	0.0085
0.90	90.071	0.1801	901.80	0.9018	9.0077	0.0090
0.95	95.033	0.1901	951.90	0.9519	9.5062	0.0095
0.99	99.046	0.1981	992.00	0.9920	9.9101	0.0099

Thus, the results of the calibration in the three ranges are shown in Figure 7a–c, where the experimental value of each of the three R_x is determined, with which the calibration adjustment was made so that the currents of the reference instrument and those of each ammeter were equal, according to their scale. The value of the slope m and its uncertainty Δ_m was obtained from the linear fit [20], one for each ammeter. Then, for the first ammeter (0–100 nA), a slope of 99.8987 nA +/−0.0519 nA was obtained; for the second (0–1 µA), a slope of 10,002.005 nA +/−0.003 nA; and finally, for the third (0–10 µA), a slope of 9.9773 µA +/−0.0175 µA. The slope value was used to obtain the experimental R_x for each ammeter, $R_x = 1/m$. The experimental values were an R_x of 10,010,236 Ω for the 0–100 nA scale ammeter, the second of 997,999 Ω for the 0–1 µA scale ammeter and the third 100,227.5 Ω for the 0–10 µA scale ammeter. To obtain the percentage uncertainty, the standard deviation of the slope is divided by the value of the slope and this result is multiplied by 100%. For the 0–100 nA scale, the ammeter has an uncertainty of +/−0.05%; for the 0–1 µA scale, the ammeter has an uncertainty of +/−0.003%; and for the 0–10 µA scale, the ammeter has an uncertainty of +/−0.17%, according to the requirements of Sections 5.2.1, 5.2.3.2, and 5.2.3.3 from the IEC 60051-2:2018, [21].

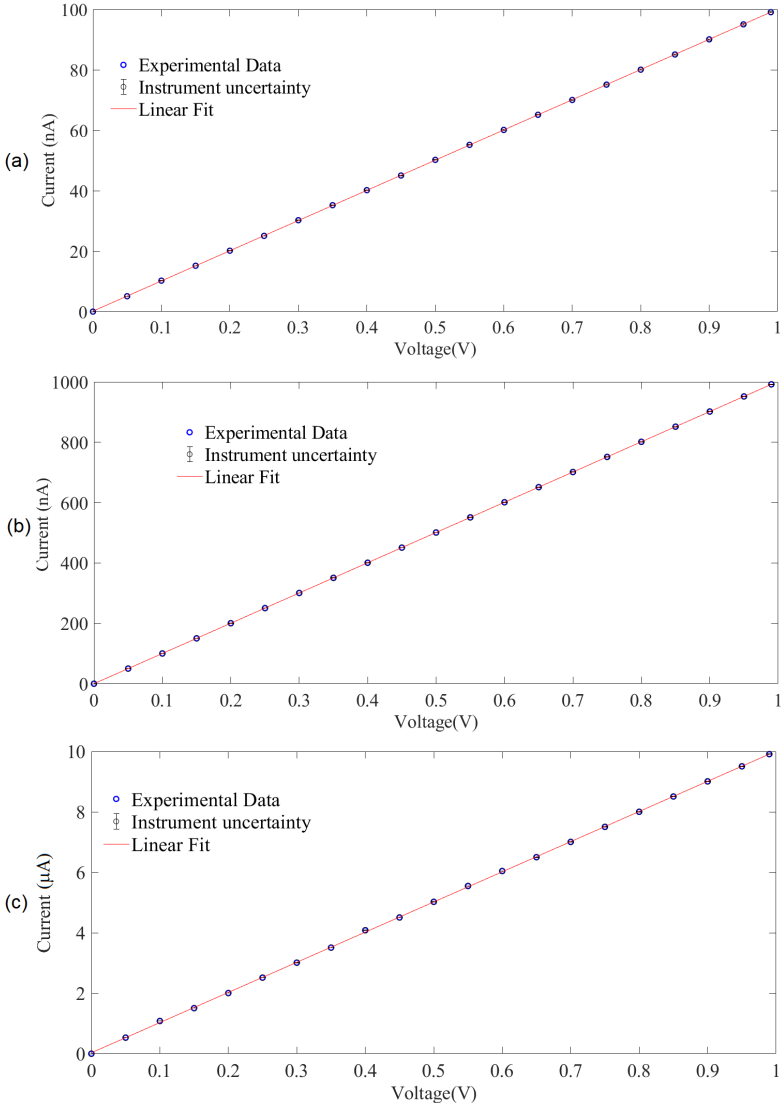

Figure 7. Calibration adjustment. (**a**) Result of the characterization of the ammeter with range from 0 to 100 nA. (**b**) Result of the characterization of the ammeter with range from 0 to 1 µA. (**c**) Result of the characterization of the ammeter with range from 0 to 10 µA.

The complete experimental setup is shown in Figure 8. Therefore, to test the current monitor, it was connected to a GEM detector. The three ammeters were placed inside a box made of double-sided printed circuit board to form a Faraday cage to decrease the external EMI.

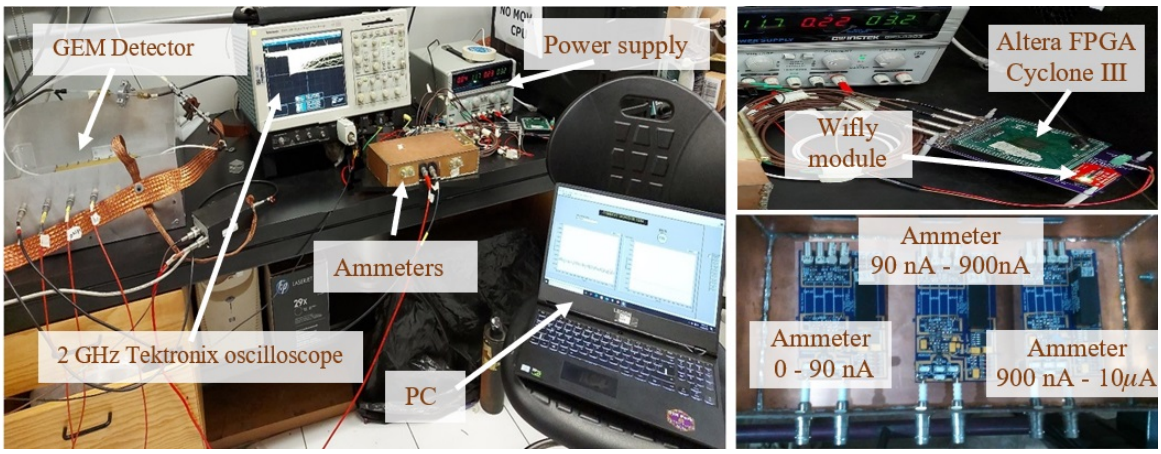

Figure 8. Experimental setup with the current monitoring system connected to the Gas Electron Multiplier (GEM).

4. Experimental Results

Tests were made to measure the current in different layers of the GEM as illustrated in Figure 9. The GEM used has 5 layers: DRIFT, TOP 1, BOTTOM 1, TOP2, and BOTTOM 2, and the current was measured in three layers: TOP 1, BOTTOM 1, and TOP 2. Below we show the measurements in these 3 layers of the ICN-UNAM GEM. The current monitoring system was connected successively to the T1, B1, and T2 electrodes to measure the currents: in the stable regime (no discharges), the behavior under discharges, and finally measured with a radioactive source (Fe 55).

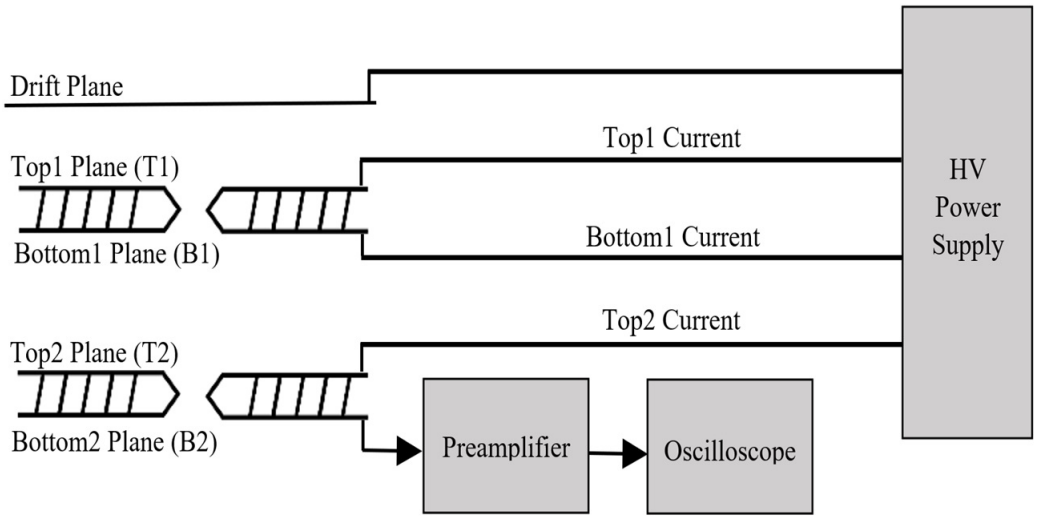

Figure 9. Block diagram of the experimental array to measure the current in the layers of the GEM.

To show the whole range of the monitor we created discharges with a current in the order of microamperes. The results of the measurements in different electrodes are shown in Figures 10–12, where results show that the ammeter performs with a maximum resolution for every current range thanks to the three-ammeter-in-one design. The ammeter operates in two different modes, i.e., it involving a single ammeter as can be seen in the figures on the left and the whole range covering from the noise in nanoamps to the spark currents in the Microamp range.

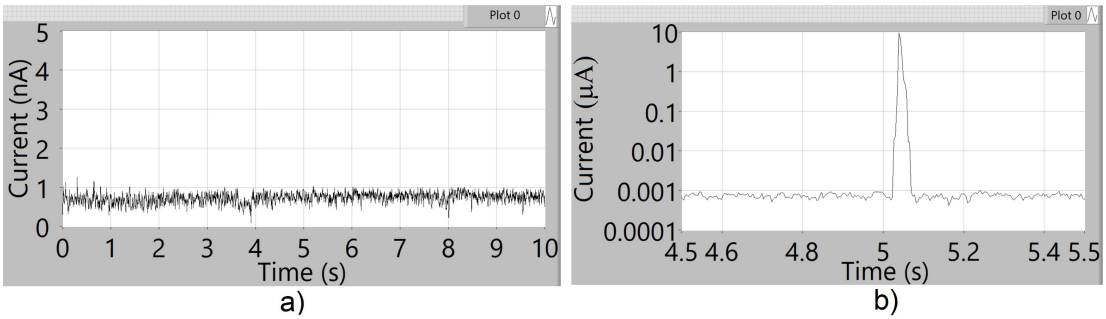

Figure 10. Current in GEM TOP 1. (**a**) Current in the stable state. (**b**) Current with a discharge, the plot shows the current in logarithmic scale.

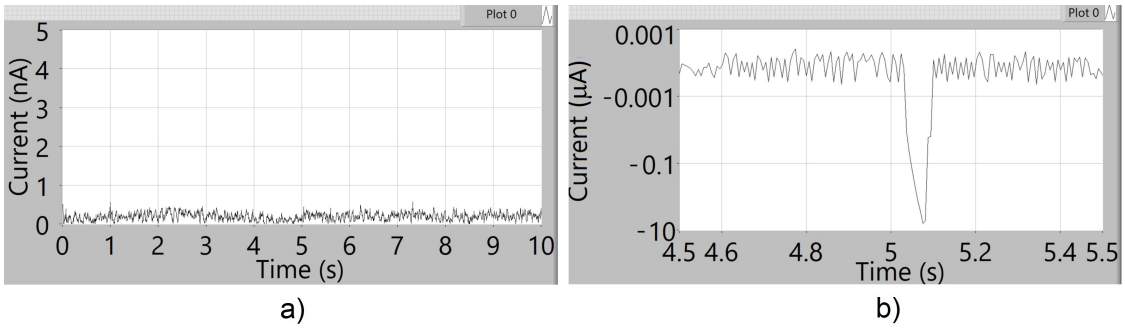

Figure 11. Current in GEM BOTTOM 1. (**a**) Current in the stable state. (**b**) Current with a discharge, the plot shows the current in logarithmic scale.

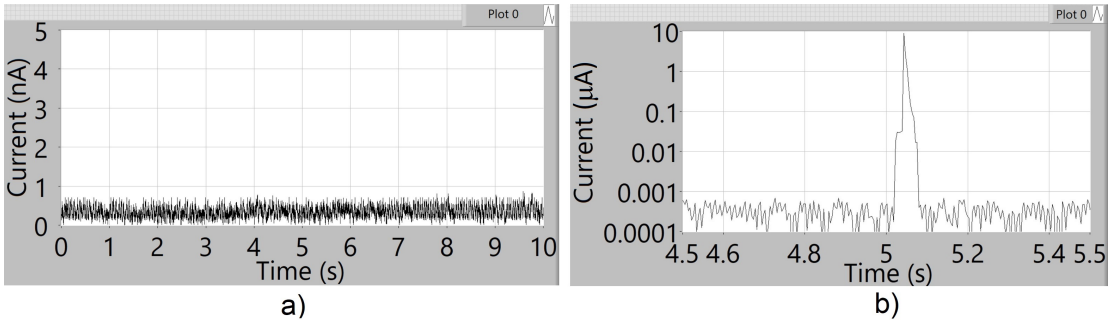

Figure 12. Current in GEM TOP 2. (**a**) Current in the stable state. (**b**) Current with a discharge, the plot shows the current in logarithmic scale.

Finally, the response of the ammeter to a feeble source of iron 55 (Fe-55) of 78.63 kBq in the center of the GEM, and the response to the radioactive source, respectively, are shown in Figures 13 and 14. Thus, a picture of the GEM´s detector is provided, as well as show the ammeter's response which was produced by the radioactive source in which displays an increment in the current, from 290 pA to 580 pA as expected.

Table 3 summarizes the research results of evaluating the responses of current in GEM for each layer. As we can see from this table the current discharge in TOP1 is positive, in BOTTOM1 is negative and in TOP2 is positive. The current in stable state in TOP1 is 750 pA, in BOTTOM1 is 220 pA, and in TOP2 is 290 pA; in these cases, there is no radiation source. The current response in GEM TOP1 and BOTTOM1 is the same with and without a radiation source; meanwhile, the responses of current in GEM TOP2 change from 290 pA to 580 pA.

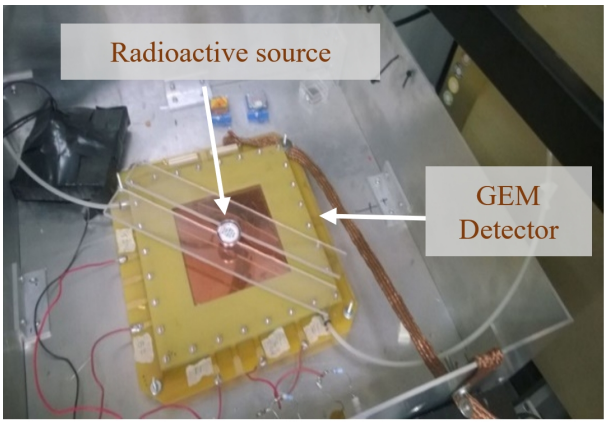

Figure 13. The (Fe-55) source on the GEM.

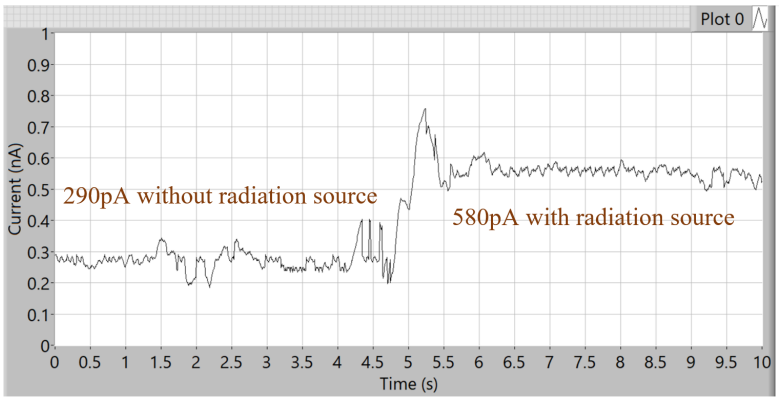

Figure 14. Current response to the radioactive source, it is shown the smoothed plot.

Table 3. Research results summarize of current in GEM layer.

GEM Layer	Current in Stable State (pA)	Current Discharge (μA)	Current with Radiation Source (pA)
TOP1	750	10	750
BOTTOM1	220	–9.8	220
TOP2	290	10	580

5. Discussion

One of the biggest and most important problems in the development of ammeters for this type of detector is that they could not be fed with conventional voltage sources as there was sufficient electromagnetic interference to prevent the GEM from working properly. It was observed that the GEM no longer generated the expected signals, but only presented a random electrical signal interpreted as noise at its output. This made it difficult to generate electrical circuits that worked properly in order to measure the current. This serious problem has been solved by combining several techniques to reduce electromagnetic interference, such as the placement of vias to divide the different sections of the PCB by building shields to reduce electromagnetic interference, the use of a Faraday cage, the placement of capacitors to produce low impedance points, and the segmentation of ground planes. It is important to note that each of these techniques by itself does not sufficiently reduce the electromagnetic interference generated by the DC-DC converter and the ADC digital signals to allow the GEM to function properly. With this, the use of batteries has been avoided and it is no longer necessary to have easy access to the current monitor, so it can be used in large arrays of GEM detectors such as those used in the Time Projection Chamber (TPC) of the A Large Ion Collider Experiment (ALICE), part of the Large Hadron Collider (LHC) of the Center for European Nuclear Research

(CERN). In these experiments, the high-voltage sources are located in specialized rooms with restricted access for security reasons where the current monitors should be installed. This current monitor could also be used in some commercial instruments to determine its degradation where it is not convenient for the user to be accidentally exposed to radiation when making a battery change.

6. Conclusions

A self-adjusting current monitoring system with a range from picoamps to 10 microamps with a 1 kHz readout was developed, using some techniques to reduce electromagnetic interference:

1. The use of vias as a shield to insulate the analog signal part from the digital one within a PCB.
2. Ground planes segmentation and capacitors as low impedance points connected to ground.

These techniques were essential to the operation of the current monitor. Notably, we were able to use optocouplers to insulate the digital part from the analog one at high voltage. Furthermore, we were able to implement the DC-DC converters to power the electronic components in the high voltage part, in spite of the important interferences they generate. The details of the design (the segmentation of the ground planes and the inclusion of electromagnetic shields in the form of vias) allowed for a considerable decrease in the interferences. The three-in-one design allows having a self-adjusting range with the optimum resolution in each range. The readout at a frequency of 1 kHz and the possibility to have a smoothed plot were implemented.

The data reading is transmitted in real-time to a PC. In future work, we may configure the module to transmit the data read in real-time via internet (IoT), which would allow the data can be stored in a cloud or shared with some other device. The data could be visualized in an app for mobile devices or on a website.

Author Contributions: All authors are involved developing the concept, simulation and experimental validation and to make the article error free technical outcome for the set investigation work. Conceptualization, S.V.-L., G.P. and M.A.D.V.-T.; methodology, S.V.-L., M.A.D.V.-T., J.L.-G. and R.S.-C.; software, S.V.-L. and R.S.-C.; validation, S.V.-L., M.A.D.V.-T., J.L.-G., G.P. and R.S.-C.; formal analysis, S.V.-L., M.A.D.V.-T., J.L.-G., G.P., R.S.-C., V.M.V.-A., F.M.-S., M.V.-T., J.G.-G. and M.E.P.-S.; investigation, S.V.-L., M.A.D.V.-T., J.L.-G., G.P., R.S.-C., V.M.V.-A., F.M.-S., M.V.-T., J.G.-G. and M.E.P.-S.; resources, S.V.-L., M.A.D.V.-T., J.L.-G., G.P., R.S.-C., V.M.V.-A., F.M.-S., M.V.-T., J.G.-G., M.E.P.-S.; S.V.-L., M.A.D.V.-T., J.L.-G., G.P., R.S.-C., V.M.V.-A., F.M.-S., M.V.-T., J.G.-G., M.E.P.-S.; writing—original draft preparation, M.A.D.V.-T., S.V.-L. and J.L.-G.; writing—review and editing, J.L.-G., M.A.D.V.-T. and S.V.-L.; visualization, M.A.D.V.-T., J.L.-G. and S.V.-L.; supervision, M.A.D.V.-T., J.L.-G. and S.V.-L.; project administration, M.A.D.V.-T., S.V.-L. and J.L.-G.; funding acquisition, S.V.-L., M.A.D.V.-T., J.L.-G., R.S.-C., V.M.V.-A., F.M.-S. and M.V.-T., J.G.-G. All authors have read and agreed to the published version of the manuscript.

Funding: This research was funded by the Programa para el Desarrollo Profesional Docente (PRODEP) in the designated project: Postdoctoral supports Consolidated and in-Consolidation academic bodies, grant number 511-6/2019-9720; and in part by the Universidad Autónoma ''Benito Juárez" de Oaxaca (UABJO).

Acknowledgments: This project was partially supported by the ESBIT-UABJO and the FCE-BUAP. R. Soto-Camacho wishes to thank the CONACYT (Consejo Nacional de Ciencia y Tecnología) for their valuable awarded a scholarship during their studies Ph.D. The authors to thank the Programa para el Desarrollo Profesional Docente (PRODEP) for funding this research. The authors wish to thank the editor and the reviewers for their valuable comments and insightful suggestions, which helped to improve this paper.

Conflicts of Interest: The authors declare no conflict of interest.

References

1. Augustinus, A.; Berger, M.; Bohmer, F.; Carena, F.; Costa, F.; Dørheim, S.; Hehner, J.; Hernandez, H.D.; Jusko, A.; Krivda, M.; et al. Readout Chambers: In ALICE TDR-016. In *Technical Design Report for the Upgrade of the ALICE Time Projection Chamber*; CERN: Meyrin, Switzerland, 2016; pp. 15–38.
2. Abelev, B.; Alice Collaboration. Upgrade of the ALICE Experiment: Letter Of intent. *J. Phys. G Nucl. Part. Phys.* **2014**, *41*, 163. [CrossRef]
3. Chernyshova, M.; Czarski, T.; Malinowski, K.; Eciwilk, E.K.; Pozniak, K.; Kasprowicz, G.; Zabołotny, W.; Wojenski, A.; Kolasinski, P.; Mazonc, D.; et al. Conceptual design and development of GEM based detecting system for tomographic tungsten focused transport monitoring: Proc. In Proceedings of the 1st EPS Conference on Plasma Diagnostics (ECPD2015) (COLL), Frascati, Italy, 14–17 April 2015; p. 240.
4. Buzulotskov, A.F. Radiation Detectors Based on Gas Electron Multipliers (Review). *Instrum. Exp. Tech.* **2007**, *50*, 283–310. [CrossRef]
5. Mindur, B.; Fiutowski, T.; Koperny, S.; Wiącek, P.; Dąbrowski, W. DAQ software for GEM-based imaging system: Proc. In Proceedings of the 20th International Workshop on Radiation Imaging Detectors (COLL), Sundsvall, Sweden, 24–28 June 2018; p. 12016.
6. Wojenski, A.; Pozniak, K.T.; Kasprowicz, G.; Kolasinski, P.; Krawczyk, R.; Zabolotny, W.; Chernyshova, M.; Czarski, T.; Malinowski, K. FPGA-based GEM detector signal acquisition for SXR spectroscopy system. *J. Instrum.* **2016**, *11*, C11035. [CrossRef]
7. Wojenski, A.; Pozniak, K.; Kasprowicz, G.; Zabolotny, W.; Byszuk, A.; Zienkiewicz, P.; Chernyshova, M.; Czarski, T. Concept and Current Status of Data Acquisition Technique for GEM Detector–Based SXR Diagnostics. *Fusion Sci. Technol.* **2016**, *69*, 595–604. [CrossRef]
8. Zabołotny, W.M.; Kasprowicz, G.; Pozniak, K.; Chernyshova, M.; Czarski, T.; Gaska, M.; Kolasin ski, P.; Krawczyk, R.; Linczuk, P.; Wojen ski, A. FPGA and Embedded Systems Based Fast Data Acquisition and Processing for GEM Detectors. *J. Fusion Energy* **2019**, *38*, 480–489. [CrossRef]
9. Sauli, F. The gas electron multiplier (GEM): Operating principles and applications. *Nucl. Instrum. Methods Phys. Res. Sect. A Accel. Spectrometers Detect. Assoc. Equip.* **2016**, *805*, 2–24. [CrossRef]
10. Deisting, A.; Garabatos, C.; Gasik, P.J.; Baitinger, D.; Berdnikova, A.; Blidaru, M.; Datz, A.; Dufter, F.; Hassan, S.; Klemenz, T.; et al. Secondary discharge studies in single and multi-GEM structures. *Nucl. Instrum. Methods Phys. Res. A* **2019**, *937*, 168–180. [CrossRef]
11. Utrobicic, A.; Kovacic, M.; Erhardt, F.; Jercic, M.; Poljak, N.; Planinic, M. Studies of the delayed discharge propagation in the Gas Electron Multiplier (GEM). *Nucl. Instrum. Methods Phys. Res. A* **2019**, *940*, 262–273. [CrossRef]
12. Yu, D.; Liu, J.; Xue, Y.; Zhang, M.; Cai, X.; Hu, J.; Dong, J.; Li, X. A 128-channel picoammeter system and its application on charged particle beam current distribution measurements. *AIP Rev. Sci. Instrum.* **2015**, *86*, 115102. [CrossRef] [PubMed]
13. Sauer, B.E.; Kara, D.M.; Hudson, J.J.; Tarbutt, M.R.; Hinds, E.A. A robust floating nanoammeter. *AIP Rev. Sci. Instrum.* **2008**, *76*, 126102. [CrossRef] [PubMed]
14. Zhou, C.-Y.; Su, H.; Mao, R.-S.; Dong, C.-F.; Qian, Y.; Kong, J. An accurate low current measurement circuit for heavy iron beam current monitor. *Nucl. Instrum. Methods Phys. Res. Sect. B Beam Interact. Mater. Atoms* **2012**, *280*, 84–87. [CrossRef]
15. Utrobicic, A.; Kovacic, M.; Erhardt, F.; Poljak, N.; Planinic, M. A floating multi-channel picoammeter for micropattern gaseous detector current monitoring. *Nucl. Instrum. Methods Phys. Res. A* **2015**, *801*, 21–26. [CrossRef]
16. Pacella, D.; Pizzicaroli, G.; Gabellieri, L.; Leigheb, M.; Bellazzini, R.; Brez, A.; Gariano, G.; Lantronico, L.; Lumb, N.; Spandre, G.; et al. Ultrafast soft x-ray two-dimensional plasma imaging system based on the Gas Electron Multiplier detector with pixel readout. *Rev. Sci. Instrum. A* **2001**, *72*, 1372–1378. [CrossRef]
17. Brahme, A.; Danielsson, M.; Iacobaeus, C.; Ostling, J.; Peskov, V.; Wallmark, M. High rate GEM detector for portal imaging. *Nucl. Instrum. Methods* **2000**, *A454*, 136–142. [CrossRef]
18. Costa, E.; Soffitta, P.; Bellazzini, R.; Brez, A.; Lumb, N.; Spandre, G. An efficient photoelectric X-ray polarimeter for the syudy of black holes and neutron stars. *Nature* **2001**, *411*, 662–665. [CrossRef] [PubMed]
19. Keithley, M. *6514 System Electrometer, Instruction Manual*; Keithley Instruments, Inc.: Cleveland, OH, USA, 2003; pp. 242–273.
20. Hastie, T.; Tibshirani, R.; Friedman, J. The Elements of Statistical Learning: Data Mining, Inference, and Prediction. In *Springer Series in Statistics*, 2nd ed.; Springer: New York, NY, USA, 2009; pp. 43–99.
21. International Standard IEC 60051-2:2018. *Direct Acting Indicating Analogue Electrical Measuring Instruments and Their Accessories—Part 2: Special Requirements for Ammeters and Voltmeters*, 5th ed.; The International Electrotechnical Commission (IEC): Geneva, Switzerland, 2018; pp. 8–33.